

# Online Navigation Planning for Long-term Autonomous Operation of Underwater Gliders

Victor-Alexandru Darvari, Charlotte Z. Reed, Jan Stratmann, Bruno Lacerda, Benjamin Allsup, Stephen Woodward, Elizabeth Siddle, Trishna Saeharaseelan, Owain Jones, Dan Jones, Tobias Ferreira, Chloe Baker, Kevin Chaplin, James Kirk, Ashley Morris, Ryan Patmore, Jeff Polton, Charlotte Williams, Alexandra Kokkinaki, Alvaro Lorenzo Lopez, Justin J. H. Buck, and Nick Hawes

**Abstract**—Underwater glider robots have become an indispensable tool for ocean sampling. Although stakeholders are calling for tools to manage increasingly large fleets of gliders, successful autonomous long-term deployments have thus far been scarce, which hints at a lack of suitable methodologies and systems. In this work, we formulate glider navigation planning as a stochastic shortest-path Markov Decision Process and propose a sample-based online planner based on Monte Carlo Tree Search. Samples are generated by a physics-informed simulator that captures uncertain execution of controls and ocean current forecasts while remaining computationally tractable. The simulator parameters are fitted using historical glider data. We integrate these methods into an autonomous command-and-control system for Slocum gliders that enables closed-loop replanning at each surfacing. The resulting system was validated in two field deployments in the North Sea totalling approximately 3 months and 1000 km of autonomous operation. Results demonstrate improved efficiency compared to straight-to-goal navigation and show the practicality of sample-based planning for long-term marine autonomy.

**Index Terms**—ocean gliders, navigation planning, Monte Carlo Tree Search, long-term autonomy

## I. INTRODUCTION

OCEAN sampling is the process of measuring indicators such as temperature, salinity, oxygen, and biomass. It is a crucial task with many applications in the sciences including biology, ecology, climatology, and meteorology. Findings based on these observations can inform policy around societal issues such as the management of the resources and ecosystems of the ocean. Ocean sampling is inherently challenging, since it involves measuring a turbulent fluid over a range of possible scales [1].

Underwater gliders, a type of autonomous underwater vehicle (AUV), are central to addressing the ocean observation problem. In contrast to *static* networks of ocean floats [2], [3], gliders allow for the sampling of *dynamic* phenomena such as eddies or ocean fronts. Gliders are able to operate autonomously for months at a time and can be much more energy-efficient and less carbon-intensive than ship operations.

Gliders now form an important part of the Global Ocean Observation System, and their activity has been increasing in the last decade [4]. It is widely accepted that their operation

Victor-Alexandru Darvari, Charlotte Z. Reed, and Nick Hawes are with the Oxford Robotics Institute, Department of Engineering Science, University of Oxford, Oxford, UK. Correspondence to [victord@robots.ox.ac.uk](mailto:victord@robots.ox.ac.uk).

The work of Jan Stratmann and Bruno Lacerda was performed while affiliated with the Oxford Robotics Institute.

All other authors are affiliated with the National Oceanography Centre, UK.



Fig. 1: Slocum glider being deployed during a preliminary experiment. The proposed *Glider Long-term Autonomy Engine (GLAE)* system was used to pilot the glider autonomously in two long-term deployments totalling approximately 3 months and 1000 km.

and management need to become more efficient in order for organisations to control increasingly large fleets of gliders [5], [6]. Standard operational procedures require input from human pilots upon the surfacing of the glider, which occurs every few hours. Pilots check weather conditions, the progress of the previous dive, and mission objectives to decide the next control instructions. This raises critical challenges as piloting supervision is not always available and the glider will continue to follow its most recent, possibly outdated, control instructions. Therefore, opportunities for optimising navigation planning are regularly lost.

A promising direction is to leverage navigation planning algorithms through autonomous command-and-control systems. Such systems can plan *online* at every surfacing given the up-to-date surfacing location and environmental conditions. Despite the existence of a fairly large body of work on navigation planning for underwater gliders (reviewed in Section II), until now such methods have not seen wide adoption for autonomous long-term missions. We argue that this is primarily due to misalignment between problem formulations and operational realities, as well as an inability to account for noise in ocean current forecasts and the execution of control commands. Furthermore, in practical terms, while existing software enables command execution and scripted missions, it does not support online replanning towards long-term mission

goals under environmental and actuation uncertainty.

In this work, we formulate the glider navigation planning problem as a stochastic shortest-path Markov Decision Process in which dives correspond to discrete decision steps and transitions are impacted by uncertainty in the currents and glider motion. Our approach combines a computationally efficient physics-based simulator that generates possible post-dive states with an online sample-based Monte Carlo Tree Search planner. These components are integrated in the *Glider Long-term Autonomy Engine (GLAE)* system, which enables online, closed-loop replanning at every surfacing. We evaluate the approach in simulation and two long-term field trials in the North Sea totalling approximately 3 months and 1000 km of autonomous operation (a photograph from a preliminary deployment is shown in Figure 1). The results demonstrate improved efficiency relative to standard navigation. To our knowledge, our work is the most extensive fully autonomous field evaluation of online glider navigation planning to date.

Our contributions are as follows:

- **MDP formulation for glider navigation planning under uncertainty.** We model multi-dive glider navigation planning as a stochastic shortest-path Markov Decision Process that explicitly accounts for uncertainty in ocean current forecasts and execution of controls.
- **A computationally efficient, physics-based dive simulator with data-driven calibration.** We design a simulator for MDP state transitions (Figure 2) that is reasonably accurate yet sufficiently fast for sample-based planning. We also propose a principled procedure for setting the simulator parameters based on a dataset of historical real-world glider dives.
- **An online sample-based planning approach for long-term marine autonomy.** We contribute an online sample-based planning technique based on Monte Carlo Tree Search (Figure 3) to solve this MDP and plan over a multi-dive horizon. The planner uses root parallelism and double progressive widening.
- **A fully integrated autonomous command-and-control system for Slocum gliders.** We implement the proposed methods in the GLAE system, which is capable of controlling commercial Slocum gliders.
- **Extensive validation.** We evaluate the approach in two North Sea campaigns totalling over 3 months and 1000 km of autonomous operation. Compared to standard navigation, in simulation we obtain gains of up to 9.88% in dive duration and 16.51% in transect length on average. We also achieve a statistically significant transect length reduction of 9.55% in a field deployment.

## II. PRIOR WORK ON GLIDER NAVIGATION PLANNING

There are two main categories of previous techniques for glider navigation planning: those based on *optimal control* and those relying on *discrete search*.

1) *Optimal Control*: In the first (and most substantial) category, an optimal control approach for planning a trajectory between two waypoints was proposed in [7], where the

problem is transformed into a nonlinear programming formulation and solved via numerical optimisation. An extension for handling time-varying currents was introduced in [8]. A path planning approach for estuarine environments (characterised by fast currents) that can optimise for both speed and energy usage was proposed in [9]. Ideas from fluid dynamic equations were combined with control theory in [10] to yield a general method for vehicles traveling through a variable flow field. Most recently, [11] proposed a method for trajectory planning for AUVs with active propulsion using high-fidelity ocean forecasts, applying it to an estuarine environment.

An overall challenge for such path planning methods is that they assume deterministic motion and environments. As a result, they cannot account for or reason about noise in the forecasts and the movement of the glider, which can lead to compounding errors. Furthermore, while they can achieve impressive performance in minimising cost to destination, this is demonstrated in simulation and not in the field. It is therefore difficult to judge how well the proposed models align with reality.

It is also worth mentioning a line of work that considers the coordination of a fleet of several gliders for achieving effective sampling. We note, however, that the objective in these works is different from planning an efficient route to a destination. A control law that allows a formation of three gliders to maintain an equilateral triangle structure was formulated in [12], which can be used to determine gradients of properties such as temperature and salinity. A general approach for the control of a mobile sensor network such as a fleet of gliders was developed in [13]. The latter method was successfully applied in the ASAP trial [14], which deployed 6 Slocum gliders over 24 days covering a total distance of 3270 km. However, this required 14 interventions from human pilots to adjust the motion patterns based on weather forecasts.

2) *Discrete Search*: In this second category of approaches, path planning using a variant of the A\* algorithm was proposed in [15]. To render the algorithm applicable, it imposes a constant dive duration and is limited to handling 2D current fields. The work in [16] is perhaps closest to ours, given that it adopts a Markov Decision Process problem formulation, considers currents across multiple depth levels, and conducts a field trial. However, a highly limiting discretisation is applied to the state space, which allows for offline planning using a value iteration algorithm. Furthermore, the field experiment is limited to a single dive.

In summary, our work is among the first to couple uncertainty-aware online navigation planning with extended real-world deployments of ocean gliders. The multi-month campaigns presented here provide one of the most extensive demonstrations to date of fully autonomous glider navigation without regular human-in-the-loop interventions.

## III. BACKGROUND

### A. Underwater Gliders

Underwater gliders [1] are AUVs that move horizontally on wings and vertically by controlling buoyancy. Descent and ascent are achieved via a piston or an artificial external bladder,

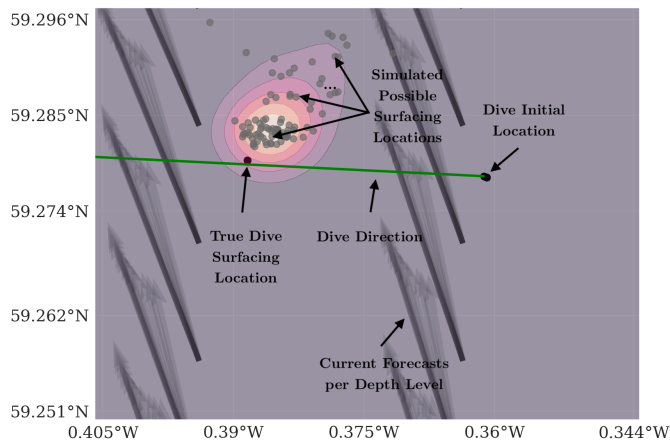


Fig. 2: An illustration of the key inputs and outputs for the glider dive simulator, which is used to generate stochastic MDP transitions.

changing the volume of the AUV but keeping mass constant. Movement is performed through *dives* consisting of several *yos*, forming a sawtooth pattern. At the start of a yo, the volume is decreased and the vehicle descends towards the ocean floor; at the bottom of each yo, the volume is increased and the vehicle ascends. The angle of the dive is controlled by shifting mass (i.e., the battery) along the internal tubing. The efficient passive propulsion of gliders renders them capable of operating for months at a time.

Gliders can be equipped with a large array of sensors for ocean sampling. Commonly used sensors include temperature, salinity, and pressure. They also feature a GPS and satellite antenna, allowing them to transmit sampled scientific data and receive control instructions. The instructions are comprised of the *waypoints* that the glider should aim to reach and the *control parameters*. Notable control parameters include the yo floor  $z_{\text{bottom}}$ , ceiling  $z_{\text{top}}$ , number of yos  $n_{\text{yos}}$ , dive pitch  $\theta_{\text{dive}}$ , climb pitch  $\theta_{\text{climb}}$ , and buoyancy change  $\chi$ . The control parameters determine the behaviour of the lower-level controller on the glider during the dive. A notable challenge is that the transfer of control instructions, which happen over satellite, are not fully reliable. Disruptions can occur in periods with adverse weather, and it is common for several transfer failures to happen in a row. The glider will use the latest set of instructions that transferred successfully, which may be significantly out of date.

Standard piloting relies on manually changing the control instructions. In between surfacings, pilots check several data sources indicating glider state and environmental factors such as wind and waves in order to prepare the next set of control instructions. Given this process occurs several times a day for months, it is not feasible for pilots to monitor every surfacing. Therefore, pilots generally set the closest waypoint such that several dives will be required to achieve it. The glider recomputes the heading towards this waypoint upon every surfacing, a mechanism we refer to as *straight-to-goal (STG)*. By diving straight towards the waypoint, opportunities are regularly lost to optimise considerations such as mission

duration (e.g., setting a heading that exploits favorable currents). This motivates our investigation of online navigation planning techniques, which can adapt to changes in glider state and environmental factors after every surfacing.

## B. MDP Preliminaries

Markov Decision Processes (MDPs) are a formalisation of decision-making [17], [18]. We define an MDP as the tuple  $(\mathcal{S}, \mathcal{A}, \mathcal{T}, \mathcal{C}, \mathcal{G})$ , where  $\mathcal{S}$  is the *state space* (all configurations the agent may find itself in),  $\mathcal{A}$  is the *action space* defining valid controls,  $\mathcal{T} : \mathcal{S} \times \mathcal{A} \times \mathcal{S} \rightarrow [0, 1]$  denotes the *transition function*, and  $\mathcal{C} : \mathcal{S} \times \mathcal{A} \times \mathcal{S} \rightarrow [0, \infty)$  is a *cost function*. Also let  $\mathcal{G} \subseteq \mathcal{S}$  denote a set of absorbing *goal states* s.t.  $\forall s_g \in \mathcal{G} \wedge s' \notin \mathcal{G}$  we have  $\mathcal{T}(s_g, a, s_g) = 1$ ,  $\mathcal{T}(s_g, a, s') = 0$ , and  $\mathcal{C}(s_g, a, s_g) = 0$ . This class of models is known as *Stochastic Shortest-Path (SSP) MDPs*.

A deterministic, stationary, Markovian policy is a mapping  $\pi : \mathcal{S} \rightarrow \mathcal{A}$ . The *value function* of such a policy for a state  $s$  is defined as  $V^\pi(s) = \mathbb{E}[\sum_{t'=0}^{\infty} C_{t'+t}^{\pi_{s'}}]$ , where  $C_{t'+t}^{\pi_{s'}}$  is a random variable denoting the cost incurred as a result of executing policy  $\pi$  starting in state  $s$  for all  $t$ . The optimal value function  $V^*$  satisfies  $V^*(s) = \min_{\pi} V^\pi(s)$ , i.e., it specifies the minimal cost attainable in expectation at each state. We seek to find the corresponding optimal policy  $\pi^*$  which, for the class of SSP MDPs, is deterministic and Markovian (i.e., independent of history given the current state) [17]. Finding or approximating  $\pi^*$  can be achieved through various MDP solution methods.

## C. MCTS for Online Planning

For many practical problems, the size of the MDP is very large [17], [19], prohibiting us from solving it exhaustively and optimally in practice. Thus, we often have to resort to solving the MDP approximately from the current state. In this work, we leverage Monte Carlo Tree Search (MCTS), an online search algorithm for determining the best action to apply at the current state of an MDP. As a full review of MCTS is out of scope, we refer the interested reader to [20] for more details.

Upper Confidence Bounds for Trees (UCT) [21] is a widely adopted MCTS algorithm. It treats action selection at each node as an independent multi-armed bandit problem, applying the principles behind the Upper Confidence Bounds (UCB) [22] algorithm to the tree search setting. UCT balances exploration of actions that have not yet been trialed with exploitation of actions that have lead to high returns. Following the principle of optimism in the face of uncertainty, the node corresponding to the action with the highest upper limit of a confidence interval on returns is chosen to be visited next.

When a node with unexplored actions is visited, MCTS creates a new node and runs a *trial* to estimate its value. The result of the trial is backpropagated towards the root of the search tree, updating the node statistics. This process is repeated until the computational budget, expressed in terms of number of trials or wall clock time, is exhausted. The depth of the search tree and quality of the MCTS solution strongly depend on the number of trials that can be ran at each planning step. When the computational budget is

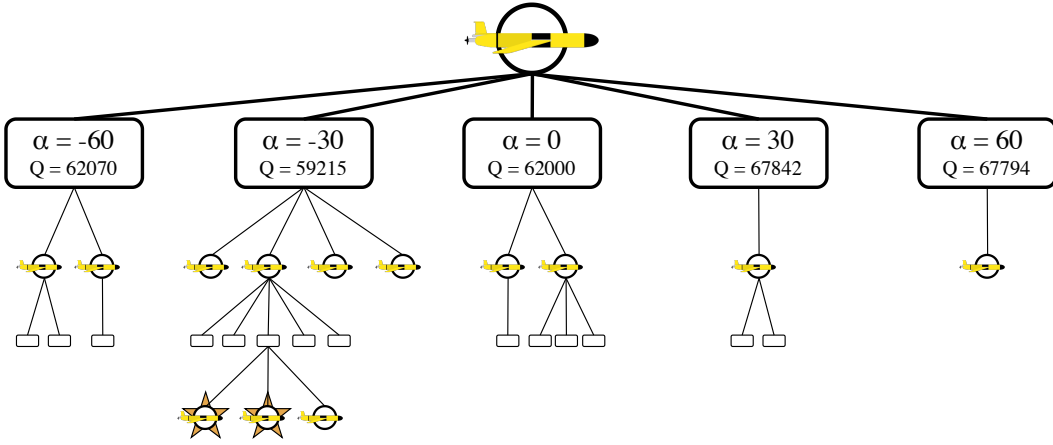


Fig. 3: An illustration of a search tree built by the planner. Circles represent state nodes and squares represent action nodes. Action nodes can have multiple children as MDP transitions  $\mathcal{T}$  are stochastic.  $Q$  is the expected cost of an action. At the root, diving at  $-30$  degrees relative to the goal is estimated to lead to the lowest expected cost. The search tree is several levels deep and explored asymmetrically by the planner to balance exploration and exploitation. Starred nodes denote terminal states in which the glider reaches the goal.

exhausted, the algorithm selects the child node of the root with the maximum visit count or best estimated value. The corresponding action will be executed in the environment.

Many variants and enhancements on the basic MCTS framework have been proposed. Notably, *double progressive widening* is suitable for scenarios characterised by stochastic transitions and continuous state spaces [23], [24]. It is able to achieve a suitable compromise between bias (induced by the first expanded nodes) and variance (in the result of trials for each state).

Parallelisation techniques have also been proposed in order to take advantage of multi-core architectures despite the sequential nature of MCTS. Notably, the *root-parallel* variant [25], [26] creates a number of search trees that progress independently from the given root state. The final results are aggregated (e.g., by majority voting) to obtain a single action.

## IV. METHODS

### A. Problem Statement

As mentioned, glider robots execute dives and surface every few hours. They *float* while transmitting scientific information and receiving control instructions, after which they *dive*. During dives, they lack the ability to communicate or localise precisely, rendering the states between dives practically unobservable. Therefore, our model of the glider navigation planning problem considers dives as discrete events. This enables us to approach the high-level navigation planning problem over a relatively long time horizon, while the control in between dives is handled by a lower-level controller on board the glider.

Let us first introduce some fundamental concepts and notation. The glider's position is represented as  $\mathbf{p} = (\lambda, \phi)$ , where  $\lambda$  and  $\phi$  denote the longitude and latitude respectively, and  $\tau$  is a continuous timestamp in seconds. A glider state is denoted as  $\mathbf{s} = (\mathbf{p}, \tau)$ . We refer to states at MDP time  $t$  as  $\mathbf{s}_t$ , and also use  $\mathbf{p}_t$  and  $\tau_t$  as shorthands. We are given a start state  $\mathbf{s}_0$  and

goal position  $\mathbf{p}_{\text{goal}}$  and seek to find a trajectory that minimises the total duration  $\Delta = \tau_T - \tau_0$  for surfacing within a radius  $\rho$  of the goal at the terminal timestep  $T$ .

Glider navigation is strongly impacted by *currents*. We represent them as the vector  $\mathbf{q}(\lambda, \phi, z, \tau) = [u, v, w]^\top$  denoting the velocity in the eastward, northward, and downward components respectively. Here,  $z$  represents the depth. The *bathymetry*  $\mathbf{b}(\lambda, \phi) = z_{\text{bathy}}$  identifies the maximum ocean depth at each position, and is relevant since gliders typically inflect when approaching the ocean floor. In contrast to currents, which we cannot measure or predict fully accurately, we may assume bathymetry is known and fixed on the timescales of the considered planning problem.

Each instance of  $I$  of the glider navigation planning problem is therefore defined as the tuple  $I = (\mathbf{p}_0, \tau_0, \mathbf{p}_{\text{goal}}, \rho, \mathbf{q}(\cdot), \mathbf{b}(\cdot))$ .

### B. MDP Formulation

To formulate the SSP MDP, we must define each element of  $(\mathcal{S}, \mathcal{A}, \mathcal{T}, \mathcal{C}, \mathcal{G})$  as introduced in Section III-B. We consider each dive as a discrete decision, and therefore the MDP time  $t$  advances by 1 with each dive.

**States.** The state space  $\mathcal{S}$  is continuous and comprises all positions  $\mathbf{p}$  and times  $\tau$  the glider may be in. In practice, these values are bounded:  $\lambda, \phi \in [-180^\circ, 180^\circ]$  while  $\tau \geq \tau_0$  and is capped by the maximum planning horizon (typically a few days).

**Actions.** Actions  $\mathcal{A}$  are defined as tuples  $\mathbf{a} = (\alpha, \mathbf{c})$ , where  $\alpha$  denotes the dive direction, while  $\mathbf{c}$  is itself a tuple consisting of the dive control parameters.

We opt to discretise the dive direction component of the action space. This allows us to inject the knowledge that small increments of heading change are largely irrelevant given the noise in the system, and avoids the challenges of working directly with a continuous action space. Furthermore,

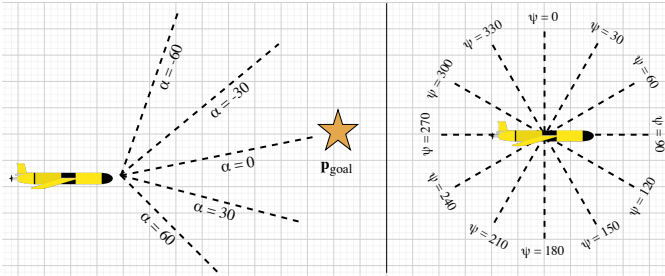


Fig. 4: Illustration of the proposed action space formulation (left), which uses bearings  $\alpha$  that are relative to the goal. This leads to a lower branching factor than deciding headings  $\psi$  directly (right) while retaining relevant actions.

we leverage the observation that glider headings  $\psi$  are set relative to the bearing  $\beta$  to the goal position  $\mathbf{p}_{\text{goal}}$ . We note the distinction between the bearing to the goal (a geometric quantity) and the vehicle heading (a control variable). Setting  $\psi = \beta$  corresponds to aiming the glider straight-to-goal which, as previously mentioned, is the default mechanism by which Slocum gliders set their heading towards a distant waypoint. Instead, we may wish to set a heading that differs from the bearing in order to account for the effect of the currents. Therefore, we allow as actions a discrete set of relative bearings  $\alpha = \beta - \psi$ . Assuming a north-east-down reference frame, positive values of  $\alpha$  correspond to diving clockwise relative to the goal, while negative values correspond to diving anti-clockwise. This preserves a lower branching factor compared to deciding the heading directly, while prioritising actions that are more likely to lead to progress towards the goal. We illustrate this in Figure 4.

**Transitions.** Transitions  $\mathcal{T}$  govern the probability of the glider surfacing in state  $\mathbf{s}_{t+1}$  after diving from state  $\mathbf{s}_t$  using action  $\mathbf{a}_t$ . In this problem, transitions are impacted by currents  $\mathbf{q}$  and noise in execution of the intra-dive control policy, and cannot be modelled fully accurately. Transitions are therefore stochastic and highly uncertain. To devise navigation plans, we thus require access to a sample-based *simulator* that can generate samples of likely surfacing states. This component is described in depth in Section IV-C.

**Costs.** The cost function  $\mathcal{C}$  we consider is  $\mathcal{C}(\mathbf{s}_t, \mathbf{a}_t, \mathbf{s}_{t+1}) = \tau_{t+1} - \tau_t$ , i.e., we incur a cost equal to the duration of the dive. Alternative cost definitions may also account for the energy usage of each set of controls; however, in our considered experimental setup, this is approximately constant.

**Goals.** The goal states  $\mathcal{G}$  are defined as  $\mathcal{G} = \{\mathbf{s} \mid d(\mathbf{p}, \mathbf{p}_{\text{goal}}) \leq \rho\}$ , where  $\rho$  is a tolerance radius and  $d$  is geodesic distance.

Regarding the impact of currents on transitions  $\mathcal{T}$ , as we cannot accurately measure and predict currents across the entire water column, we must rely on forecasts  $\hat{\mathbf{q}}$ . Many ocean models exist, which vary in accuracy as well as spatial and temporal resolutions. Such models employ discretisation by splitting coordinates, depth, and time into intervals. Concretely, as we focus our deployment and evaluation in the North Sea region, we make use of the AMM15 [27] model, which provides forecasts at hourly intervals, over 33 depth

levels, and over grid cells of approximately  $1.5\text{km} \times 1.5\text{km}$ . We obtain these forecasts via the Met Office marine data service [28]. These forecasts have a horizon of 5 days. This model does not include vertical speeds; therefore, we assume  $w = 0$ , i.e.,  $\hat{\mathbf{q}}(\lambda, \phi, z, \tau) = [u, v, 0]^T$ .

### C. Custom Glider Dive Simulator

Our approach requires a *simulator* that can generate samples from the transition function  $\mathcal{T}$ . The simulator must balance the accuracy of sampled transitions with execution speed. As mentioned in Section III-C, the number of trials that can be ran in a fixed computational budget strongly influences MCTS performance. Constructing a search tree over a horizon of several dives is crucial for going beyond reactive current correction.

The best available open source simulator for Slocum gliders is `glidersim` [29]. This state-of-the-art approach is highly detailed and takes into account glider actuator behaviour as well as the hydrodynamics of Slocum gliders [30], [31]. However, this comes at the expense of costly runtime. The method also does not account for the unknowns surrounding the current forecasts and it is unsuitable for use in our approach. Thus, we set out to devise a custom simulator.

To design a faster simulator more appropriate for sample-based planning methods, we leverage the following observations. Firstly, the majority of large-scale, publicly available ocean models (including AMM15) do not include vertical speeds. As such, we cannot use forecasts to account for vertical influences on the glider’s depth rate, and we can treat it as approximately constant. Secondly, the glider moves in a largely steady-state (i.e., constant speed and attitude relative to the water) when performing the sawtooth motion. This is not the case at the bottom and top of each yo, when the onboard controller changes the glider pose and velocity. Nevertheless, these transient phases can be considered negligible in terms of the impact on the overall trajectory. This motivates our simulation approach that chains together steady-state segments.

The pseudocode for our custom glider dive simulator is given in Algorithm 1. The *inputs* to the simulator are the glider state  $\mathbf{s}$ , action  $\mathbf{a}$ , bearing  $\beta$ , current forecasts  $\hat{\mathbf{q}}$  and bathymetry  $\mathbf{b}$ . The *output* of the simulator is the post-dive state  $\mathbf{s}'$ . We note that, unlike in the MDP states described in Section IV-B, in which the glider is always at the surface, the internal glider states in the simulator also contain a depth level. We denote this internal state as  $\mathbf{g}$ . Querying the forecast and bathymetry is denoted  $\hat{\mathbf{q}}(\mathbf{g})$  and  $\mathbf{b}(\mathbf{g})$ .

The main loop of the algorithm (`SimulateDive`) simulates the characteristic seesaw-like motion by chaining together upwards and downwards steady-state phases (`SteadyUp` and `SteadyDown`) until the number of yos to perform is exhausted. The `SteadyDown` method simulates a downward steady-state phase by repeatedly propagating the glider to the next forecast cell. The `SteadyUp` method does the same except with the glider moving upwards. The general idea is that, as the forecast currents are constant in a grid cell, the glider state can be propagated linearly within that cell until the cell border is hit (`TimeToNextCell`). Glider horizontal speed

**Algorithm 1** Custom Glider Dive Simulator

---

```

1: Parameters:  $\Theta = \{\theta_{\text{drag}_i}, \theta_{\text{drag}_j},$ 
    $\theta_{\text{curr\_mag}}, \theta_{\text{curr\_dir}}, \theta_{\text{curr\_min}},$ 
    $\theta_{\text{motion\_mag}}, \theta_{\text{motion\_dir}}, \theta_{\text{motion\_min}}\}$ 
2: Function SimulateDive( $\mathbf{s}, \mathbf{a}, \beta, \hat{\mathbf{q}}, \mathbf{b}$ ):
3:    $(\mathbf{p}', \tau') \leftarrow \mathbf{s}$ 
4:   halfYosDone  $\leftarrow 0$ 
5:   while halfYosDone  $< 2 * \mathbf{a.c.n}_{\text{yos}}$  do
6:     if halfYosDone mod 2 = 0 then
7:        $(\mathbf{p}, \tau) \leftarrow \text{SteadyDown}(\mathbf{s}, \mathbf{a}, \beta, \hat{\mathbf{q}}, \mathbf{b})$ 
8:     else
9:        $(\mathbf{p}, \tau) \leftarrow \text{SteadyUp}(\mathbf{s}, \mathbf{a}, \beta, \hat{\mathbf{q}}, \mathbf{b})$ 
10:    end if
11:    halfYosDone += 1
12:  end while
13:   $\mathbf{s}' = (\mathbf{p}, \tau)$ 
14:  return  $\mathbf{s}'$ 

15: Function SteadyDown( $\mathbf{s}, \mathbf{a}, \beta, \hat{\mathbf{q}}, \mathbf{b}$ ):
16:   $\psi \leftarrow \text{HeadingFromAction}(\mathbf{a}, \alpha, \beta)$ 
17:   $s, w_g \leftarrow \text{GliderFlightModel}(\mathbf{a}, \mathbf{c})$ 
18:   $u_g, v_g \leftarrow s \cdot \sin \psi, s \cdot \cos \psi$ 
19:   $u_g, v_g \leftarrow \text{ApplyMotionNoise}(u_g, v_g)$ 
20:   $\mathbf{g} \leftarrow [\mathbf{p}, z, \tau]^\top$ 
21:   $\dot{\mathbf{g}} \leftarrow [u_g, v_g, -w_g]^\top$ 
22:  while  $\mathbf{g}[2] > \min(\mathbf{a.c.z}_{\text{bottom}}, \mathbf{b}(\mathbf{g}))$  do
23:     $\mathbf{g} \leftarrow \text{ToNextCell}(\hat{\mathbf{q}}, \mathbf{g}, \dot{\mathbf{g}}, \mathbf{a.c.z}_{\text{bottom}})$ 
24:  end while
25:   $(\mathbf{p}', \tau') \leftarrow (\mathbf{g}[1], \mathbf{g}[3])$ 
26:  return  $(\mathbf{p}', \tau')$ 

27: Function ToNextCell( $\hat{\mathbf{q}}, \mathbf{g}, \dot{\mathbf{g}}, z_{\text{lim}}$ ):
28:   $u, v, _ \leftarrow \hat{\mathbf{q}}(\mathbf{g})$ 
29:   $\hat{\mathbf{q}}(\mathbf{g}) \leftarrow \text{GetNoisyCurrents}(u, v)$ 
30:   $\dot{\mathbf{g}}_{\text{true}} \leftarrow \text{ApplyCurrAccel}(\dot{\mathbf{g}}, \hat{\mathbf{q}}(\mathbf{g}), \theta_{\text{drag}_i}, \theta_{\text{drag}_j})$ 
31:   $\Delta\tau \leftarrow \text{TimeToNextCell}(\hat{\mathbf{q}}, \mathbf{g}, \dot{\mathbf{g}}_{\text{true}}, z_{\text{lim}})$ 
32:   $\mathbf{g} \leftarrow \mathbf{g} + \dot{\mathbf{g}}_{\text{true}} \cdot (\Delta\tau + \varepsilon)$ 
33:  return  $\mathbf{g}$ 

34: Function SteadyUp( $\mathbf{s}, \mathbf{a}, \beta, \hat{\mathbf{q}}, \mathbf{b}$ ):
35:  /* Similar to SteadyDown but with  $+w_g$  in  $\dot{\mathbf{g}}$  and
   condition  $\mathbf{g}[2] < \mathbf{a.c.z}_{\text{top}}$  */

36: Function TimeToNextCell( $\hat{\mathbf{q}}, \mathbf{g}, \dot{\mathbf{g}}_{\text{true}}, z_{\text{lim}}$ ):
37:  /* Calculates time until next cell of forecast  $\hat{\mathbf{q}}$  is reached
   using geographical distances and glider speed  $\dot{\mathbf{g}}_{\text{true}}$ . */

38: Function GetNoisyCurrents( $u, v$ ):
39:   $|q| \leftarrow \sqrt{u^2 + v^2}, \alpha_{\text{curr}} \leftarrow \text{atan}(v, u)$ 
40:   $\text{magN} \sim \mathcal{N}(0, \theta_{\text{curr\_mag}}), \text{dirN} \sim \mathcal{N}(0, \theta_{\text{curr\_dir}})$ 
41:   $|q| \text{ += magN}, \alpha_{\text{curr}} \text{ += currN}$ 
42:   $|q| = \max(|q|, \theta_{\text{curr\_min}})$ 
43:  return  $\text{polarToVec}(|q|, \alpha_{\text{curr}})$ 

44: Function ApplyMotionNoise( $u, v$ ):
45:  /* Similar to GetNoisyCurrents but with magN
   and dirN generated using random walks with parameters
    $\theta_{\text{motion\_mag}}, \theta_{\text{motion\_dir}}$  and minimum speed  $\theta_{\text{motion\_min}}$ . */

```

---

$s \in \mathbb{R}^+$  and vertical speed (depth rate)  $w_g \in \mathbb{R}^+$  are calculated (GliderFlightModel) using the approach of Merckelbach *et al.* [31]. This takes into account the control parameters in  $\mathbf{c}$  as well as water properties. The flight model parameters are fit to historical glider data from the region of interest. Acceleration is applied to the glider speeds as determined by the current forecast and drag coefficients  $\theta_{\text{drag}_i}, \theta_{\text{drag}_j}$  that are part of the simulator parameters.

By default, transitions  $\mathcal{T}$  generated by this simulator would be deterministic. However, as we would like the produced navigation plans to be robust to forecast and control errors, we inject two types of noise in order to yield several plausible samples of stochastic transitions given the same inputs. Namely, we inject *current noise* and *motion noise*.

We use a simple Gaussian noise model for the current noise (GetNoisyCurrents). Independent noise is added to the magnitude and direction by sampling from Gaussian distributions with mean 0 and configurable standard deviations  $\theta_{\text{curr\_mag}}, \theta_{\text{curr\_dir}}$ . These perturbations are applied consistently for all forecasts  $\hat{\mathbf{q}}$  given a particular random seed, corresponding to a systematic bias in the forecast.

To implement motion noise (ApplyMotionNoise), we update the glider velocity with a random walk to reflect the noise of the internal dead-reckoning characterised by a very inaccurate state estimation and other local perturbations – a noise model suggested by glider pilots. We simulate a symmetric random walk over integers with absorbing barriers for which the probability of the value decreasing, staying put, or increasing is uniform. Separate walks are used for the magnitude and direction. The values of the random walk states are multiplied with the  $\theta_{\text{motion\_mag}}$  and  $\theta_{\text{motion\_dir}}$  noise parameters then added to the glider magnitude and direction.

The simulator parameters  $\Theta$ , enumerated in Line 1 of Algorithm 1, control the impact of the currents on glider speed and the amount of noise that is injected into the simulator. As these parameters are challenging to establish a priori and depend significantly on the deployment vehicle, location, and conditions, we propose a procedure to tune them using past glider data. We describe this procedure in the next section.

#### D. Simulator Parameter Tuning

Choosing the simulator parameters  $\Theta$  appropriately is of crucial importance for ensuring the fidelity of the generated transitions from  $\mathcal{T}$  and, consequently, the effectiveness of the generated navigation plans. We denote an instance of the simulator parameterised with a particular  $\Theta$  as  $\mathcal{T}_\Theta$ .

To enable tuning  $\Theta$ , we assume availability of a dataset  $\mathcal{D} = \{\mathbf{x}^{(i)}\}_{i=1}^N$  of historical dives with entries  $\mathbf{x}^{(i)}$  of the form  $((\mathbf{s}^{(i)}, \mathbf{a}^{(i)}, \beta^{(i)}, \hat{\mathbf{q}}^{(i)}, \mathbf{b}^{(i)}), \mathbf{s}_{\text{true}}^{(i)})$ , comprising the conditions prior to starting a dive and the true post-dive state after the glider surfacing. For simplicity, we also assume that all parameters  $\mathbf{c}$  except  $n_{\text{yos}}$  and  $z_{\text{bottom}}$  are held constant within a dataset used to fit the simulator parameters.

We focus on optimising the generated simulator positions relative to the ground truth  $\mathbf{p}_{\text{true}}^{(i)}$ , as durations  $\tau' - \tau$  can realistically be treated as approximately constant given our assumption of fixed control parameters.

For each  $\mathbf{x}^{(i)}$ , we draw  $M$  samples of future states  $\mathbf{s}^{(i,1)}, \mathbf{s}^{(i,2)}, \dots, \mathbf{s}^{(i,M)} \sim \mathcal{T}_\Theta(\mathbf{s}, \mathbf{a}, \beta, \hat{\mathbf{q}}, \mathbf{b})$ , and record the positions  $\mathcal{P}^{(i)} = \{\mathbf{p}^{(i,1)}, \mathbf{p}^{(i,2)}, \dots, \mathbf{p}^{(i,M)}\}$ . We subsequently fit a per-dive KDE with a Gaussian kernel  $\hat{p}_\Theta^{(i)} = KDE(\mathcal{P}^{(i)}; h)$  with bandwidth parameter  $h$ . Evaluating the probability  $\hat{p}_\Theta^{(i)}(\mathbf{p}_{\text{true}}^{(i)})$  of the true surfacing location under the KDE gives us a score quantifying how well the simulator parameters  $\Theta$  fit a particular dive. Furthermore, we also penalise the spread  $\sum_{j=1}^M (\mathbf{p}^{(i,j)} - \overline{\mathbf{p}}^{(i,j)})^2$  of the positions relative to their mean. The scoring function  $J(\Theta)$  is therefore defined as:

$$J(\Theta) = \sum_{i=1}^N \log \hat{p}_\Theta^{(i)}(\mathbf{p}_{\text{true}}^{(i)}) - \lambda_{\text{reg}} \sum_{i=1}^N \sum_{j=1}^M (\mathbf{p}^{(i,j)} - \overline{\mathbf{p}}^{(i,j)})^2,$$

where the first term corresponds to the log-likelihood  $\ell(\Theta; \mathcal{D})$  and the second term penalises the spread of samples generated for each  $\mathbf{x}^{(i)}$  with a configurable weight  $\lambda_{\text{reg}}$ .

We seek to find the optimal parameters  $\Theta^* = \text{argmax}_\Theta(J(\Theta))$ . This is a high-dimensional optimisation problem with a scoring function that is expensive to evaluate and cannot be computed in closed form. As such, Bayesian optimization is a suitable framework. Concretely, we opt for BoTorch [32], [33], whose acquisition function navigates the exploration-exploitation tradeoff to generate promising candidate parameter sets  $\Theta_k$  at each iteration  $k$  of a total  $n_{\text{SIM-BO}}$  iterations.

### E. Sample-Based Online Planner

Gliders surface every few hours and await instructions for the next dive while uploading scientific data. Thus, an *online* planning approach is natural for solving this MDP, leveraging this time to derive a navigation plan. At each surfacing, the problem instance  $I = (\mathbf{p}_0, \tau_0, \mathbf{p}_{\text{goal}}, \rho, \mathbf{q}(\cdot), \mathbf{b}(\cdot))$  is assembled using the position  $\mathbf{p}_0$  from the glider's GPS fix, time  $\tau_0$ , goal specification, current forecasts, and bathymetry.

The online setup coupled with the sample-based nature of the simulator  $\mathcal{T}_\Theta$  means UCT with double progressive widening is an appropriate choice. We note that, despite the discretisation of the actions, we opt for progressive widening in the action space also. This is done to maintain the branching factor low and increase the tree depth, enabling us to plan over a longer horizon.

Planning is carried out while the glider is at the surface using  $n_{\text{trials}}$  samples, a parameter that is set on a per-deployment basis to account for the expected time duration of the glider at the surface and the computational resources available. As UCT is sequential, we opt for the root-parallel variant to aggregate results from  $n_{\text{threads}}$  runs, improving the robustness of the navigation plan to noise in the current forecasts and action choices early in the tree search. Pseudocode for the algorithm is given in Algorithm 2. We highlight the following differences from a standard implementation:

- **Use of heuristic.** We do not perform rollouts to estimate the value of leaf nodes as transitions require running a physics-based simulation. Instead, we use a heuristic (line 19) that estimates the time to reach the goal based on

---

### Algorithm 2 Sample-Based Online Planner

---

```

1: Function PlanNextDive( $I$ ):
2:   allActions  $\leftarrow []$ 
3:   for each  $j$  out of  $n_{\text{threads}}$  in parallel
4:     seed  $\leftarrow$  SampleRandomState( $j$ )
5:     action  $\leftarrow$  RunUCT( $I$ , seed)
6:     allActions.Append(action)
7:   end for
8:    $\mathbf{a} \leftarrow$  MajorityVote(allActions)
9:   return  $\mathbf{a}$ 
10: Function RunUCT( $I$ , randomState):
11:    $(\mathbf{p}_0, \tau_0, \mathbf{p}_{\text{goal}}, \rho, \mathbf{q}(\cdot), \mathbf{b}(\cdot)) \leftarrow I$ 
12:   create root node  $v_{\text{root}}$  from  $s_0 = (\mathbf{p}_0, \tau_0)$ 
13:   for  $i$  in  $[1, n_{\text{trials}}]$  do
14:      $v_{\text{leaf}} \leftarrow$  TreePolicy( $v_{\text{root}}$ )
15:      $\mathbf{s} \leftarrow$  GetState( $v_{\text{leaf}}$ )
16:     if  $\mathbf{s} \in \mathcal{G}$  then
17:        $r \leftarrow$  SumCosts( $\mathbf{s}_0, \mathbf{s}$ )
18:     else
19:        $r \leftarrow \epsilon_{\text{heur}} * (d(\mathbf{p}, \mathbf{p}_{\text{goal}})/s)$ 
20:     end if
21:     Backup( $v_{\text{leaf}}, r$ )
22:   end for
23:   action  $\leftarrow$  RobustChild( $v_{\text{root}}$ )
24:   return action

```

---

the current distance and constant speed. The error term  $\epsilon_{\text{heur}}$  of the heuristic was calibrated based on preliminary deployment data and was set to approximately 1.77. Equivalently, the typical trajectory length was  $1.77 \times$  that of the straight line.

- **Prioritising STG action.** When expanding a node, we always add the child corresponding to the STG action ( $\alpha = 0$ ) first. Further actions are sampled randomly from  $\mathcal{A}$  as visit counts increase and the progressive widening condition is triggered. This prioritises an action that leads to good returns in most situations and corresponds to the standard navigation baseline.

## V. GLIDER LONG-TERM AUTONOMY ENGINE

In this section, we describe the components required for translating our methodological and algorithmic contributions discussed in the previous section to a field-validated system that performs long-term autonomous navigation planning for underwater gliders. The *Glider Long-term Autonomy Engine* system was designed and implemented in collaboration with glider pilots and marine robotics stakeholders in order to promote operational practicality and safety. The system as described herein is currently compatible with Slocum gliders [34], [35] and is in principle extensible to other designs such as Seaglider [36].

### A. Automated Goal Management

The previous section specified problem instances  $I$  with a single goal  $\mathbf{p}_{\text{goal}}$ . However, glider missions typically consist of many such goals. A common use case, which we target,

**Algorithm 3** Converting the output of the online planning algorithm to a list of waypoints as required by Slocum gliders.

```

1: Function ToWptList( $\alpha, \mathbf{p}_0, \mathbf{p}_{\text{goal}}^{\text{curr}}, \mathbf{p}_{\text{goal}}^{\text{next}}, \rho, \rho_{\text{wpt}}, n_{\text{bck}}$ ):
2:   wpts  $\leftarrow$  []
3:   goal_d  $\leftarrow$   $d(\mathbf{p}_0, \mathbf{p}_{\text{goal}}^{\text{curr}})$ 
4:   if goal_d  $<$   $\rho_{\text{wpt}}/2$  then
5:     wpts.append( $\mathbf{p}_{\text{goal}}^{\text{curr}}$ )
6:   else
7:     wpt_d  $\leftarrow$   $\min(\text{goal\_d}, \rho_{\text{wpt}})$ 
8:      $\beta$  = getBearing( $\mathbf{p}_0, \mathbf{p}_{\text{goal}}^{\text{curr}}$ )
9:      $\psi$   $\leftarrow$   $\beta - \alpha$ 
10:    wpt  $\leftarrow$  pointOnHeading( $\mathbf{p}_0, \psi, \text{wpt\_d}$ )
11:    wpts.append(wpt)
12:  end if
13:  addBackupWpts(wpts,  $\mathbf{p}_{\text{goal}}^{\text{curr}}, \rho, \rho_{\text{wpt}}, n_{\text{bck}}$ )
14:  addBackupWpts(wpts,  $\mathbf{p}_{\text{goal}}^{\text{next}}, \rho, \rho_{\text{wpt}}, n_{\text{bck}}$ )
15: Function addBackupWpts(wpts,  $\mathbf{p}_{\text{goal}}^{\text{bck}}, \rho, \rho_{\text{wpt}}, n_{\text{bck}}$ ):
16:  while len(wpts)  $\leq$   $n_{\text{bck}}$  do
17:     $\mathbf{p}$   $\leftarrow$  wpts[-1]
18:    if  $d(\mathbf{p}, \mathbf{p}_{\text{goal}}^{\text{bck}})$   $<$   $\rho$  then
19:      break
20:     $\beta$  = getBearing( $\mathbf{p}, \mathbf{p}_{\text{goal}}^{\text{bck}}$ )
21:    wpt  $\leftarrow$  pointOnHeading( $\mathbf{p}, \beta, \rho_{\text{wpt}}$ )
22:    if overshootsGoal(wpt,  $\mathbf{p}_{\text{goal}}^{\text{bck}}, \rho$ ) then
23:      wpt  $\leftarrow$   $\mathbf{p}_{\text{goal}}^{\text{bck}}$ 
24:    wpts.append(wpt)
25:  end while

```

is to have the glider sample data between a set of predefined points, i.e., a *transect* in the case of two points and the corners a polygon more generally. We therefore assume we are given an ordered list of points  $\{\mathbf{p}_{\text{goal}}^{(i)}\}_{i=1}^{n_{\text{goals}}}$ . The system advances to the next goal in the list upon achieving the present one, and cycles to the beginning of the list once the end is reached.

### B. Waypoint List Generation

A *waypoint list* specifies an ordered sequence of waypoints that the glider should achieve. Waypoint lists are the first file type required for translating an action  $\mathbf{a} = (\alpha, \mathbf{c})$  output by the planner to files that can be understood by a Slocum glider. While the action space of the planner is formulated in terms of relative bearings (Section IV-B), the Slocum glider expects a list of *waypoints*. A suitable translation approach is therefore needed.

As mentioned in Section III-A, several failures in transferring control instructions can occur in a row. Therefore, providing a single close waypoint is insufficient. From an operational standpoint, waypoint lists must extend well beyond a single dive so that the vehicle can continue its mission uninterrupted in the case of communication failures. The approach we propose uses the planner action to compute the first waypoint and several backup waypoints derived using straight-to-goal bearings. Since waypoint lists are recomputed and updated at each surfacing, this allows the vehicle to steer according to planner output during normal operation, and use a sensible backup trajectory otherwise.

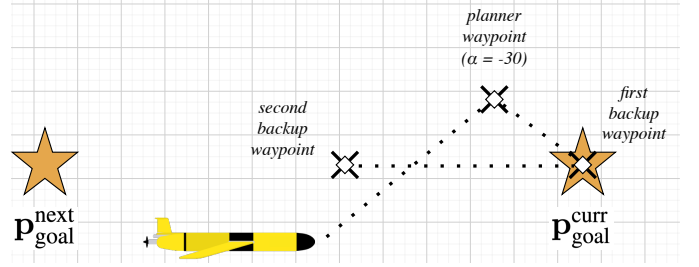


Fig. 5: Visualisation of waypoint list generation. The first waypoint corresponds to the planner action (here,  $\alpha = -30$ ). The first backup waypoint is set to be the current goal as otherwise the goal would be overshoot. The second backup waypoint is aimed straight at the next goal.

Pseudocode for the waypoint list conversion procedure is given in Algorithm 3 and an example is shown in Figure 5. The algorithm takes as input the action  $\alpha$ , glider position  $\mathbf{p}_0$ , the position of the current goal  $\mathbf{p}_{\text{goal}}^{\text{curr}}$ , that of the next goal  $\mathbf{p}_{\text{goal}}^{\text{next}}$ , the goal tolerance radius  $\rho$ , the waypoint distance  $\rho_{\text{wpt}}$ , and number of backup waypoints  $n_{\text{bck}}$ .

The algorithm first determines the waypoint corresponding to the planner action (lines 3-12). If distance to the goal is low, the goal itself is used as the waypoint to avoid repeatedly oscillating around it. Otherwise, the waypoint is set along the heading of the planner action at the specified waypoint distance. Backup waypoints towards the current goal and, if required, the next goal (lines 13-14) are added.

The bearings for the backup waypoints are computed starting from the last waypoint (line 17). Additional backup waypoints towards a particular goal are not necessary if the previous waypoint is already within the same goal region (lines 18-19), and this serves as the loop termination condition. As mentioned, the bearing to the goal is used as the heading for the backup waypoints. If a backup waypoint overshoots the goal region, it is replaced with the goal itself (lines 22-23).

### C. Underwater Goal Achievement Detection

Regarding determining whether the goal was achieved, i.e., whether  $\mathbf{s} \in \mathcal{G}$ , there is an additional condition that must be checked in GLAE besides the dive surfacing within the goal region. The additional condition is necessary to align our problem formulation with operational characteristics of Slocum gliders, which detect whether a waypoint was achieved while underwater using dead reckoning (which we note may be inaccurate). As the waypoint matches the goal itself when approaching the goal region (see previous section), the glider may start automatically advancing towards the next goal while underwater.

Concretely, if the waypoint is deemed achieved underwater, the glider switches mid-dive to the next waypoint in the navigation plan. As the glider reports the waypoint it is following upon every surfacing, the position of the waypoint in the last navigation plan can be used to check if this condition is met. GLAE advances to the next goal in the ordered list if either this condition *or* the surfacing within the goal region condition is met.

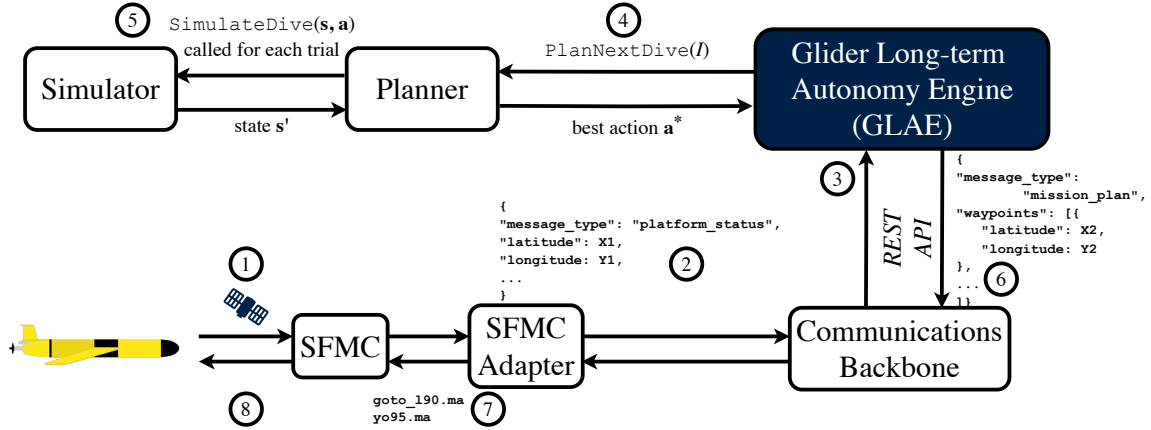


Fig. 6: Flow diagram illustrating the components and steps for online planning. This workflow is executed every few hours upon the surfacing of the glider.

#### D. Instruction Set Generation

The second file type required, the *instruction set*, contains the dive control parameters  $c$ . Following the guidance of glider pilots, GLAE supports specifying a number of fixed instruction sets  $\mathcal{K}$  that determine the vehicle speed, sampling speed, and other operational variables. This ensures the control parameters that can be output by GLAE are within a field-tested, pre-approved range of configurations.

As previously mentioned, for simplicity, we assume that a fixed set of control parameters  $c$  is used for the duration of a particular mission. This assumption is realistic for the deployments considered in our evaluation, which require sampling of scientific data at regular time and distance intervals, and thus a fixed  $c$  is highly appropriate, as is also used in the field. A choice of a particular instruction set  $c \in \mathcal{K}$  corresponding, for example, to medium vehicle speed and high data sampling rates is specified when a mission is initialised.

#### E. System Components and Integration

Besides GLAE, several components are required to achieve the full control loop of the glider. This is made possible by integration with the Oceanids C2 infrastructure [37] built by the UK National Oceanography Centre (NOC). This platform provides the necessary components to achieve real-time ingestion of vehicle information and transfer of control instructions using standardised interfaces. In this section, we describe the system components and how they are integrated.

**Glider Long-term Autonomy Engine.** The GLAE system contributed in this paper implements the methodology described in Section IV and is set up as a service deployed to on-premise computational infrastructure. It is capable of controlling several gliders simultaneously. GLAE fetches the most recent current forecasts from Copernicus or the Met Office Marine Data Service daily once they are published to inform navigation planning.

**C2 Communications Backbone.** This open-source component [38] provides publish-subscribe functionality. It is powered by a RabbitMQ message queue. A variety of clients can read and write messages in a suite of standardised formats [39]

via HTTP APIs that are access-controlled. In the remainder of this section, we indicate specific message formats from this repository using monospace font (e.g., `platform_status`). **SFMC Adapter.** The Slocum Fleet Mission Control (SFMC) Adapter is a microservice that converts between the standardised formats of the Communications Backbone and the specific file formats required by Slocum gliders.

**SFMC.** This proprietary component is the software suite created by the Slocum glider manufacturer. It provides interfaces for controlling the glider, either manually via a terminal or programmatically using APIs. It enables transferring files containing waypoints and control parameters to the glider by placing them in a dedicated directory from which they are read. SFMC communicates with gliders directly via an Iridium satellite link.

**C2 Piloting User Interface.** This web-based interface can be used to configure missions for, monitor, and pilot marine autonomous systems. It is complementary to the SFMC web-based interfaces and unifies piloting interfaces for a variety of platforms beyond Slocum gliders [37].

#### F. Workflows

Next, we describe the two main workflows. The Mission Configuration Workflow is higher-level and executed once at the start of a mission. The Online Planning Workflow is lower-level and executed after every glider surfacing in order to provide up-to-date control instructions so as to best achieve the mission goals.

**Mission Configuration Workflow.** The workflow to configure a glider mission involves the use of the C2 Piloting UI to indicate the glider for the mission, the list of goals  $[p_{\text{goal}}^{(i)}]$ , and permitted instruction sets  $\mathcal{K}$ . A `planning_configuration` message is generated and published to the Backbone. The GLAE system, upon receiving the message, initialises the tracking information in persistent storage. From this point onwards, GLAE will track the mission goals and respond to post-surfacing updates from the glider with navigation plans.

**Online Planning Workflow.** This workflow achieves the full glider control loop. The steps are illustrated in Figure 6,

wherein the numbers above the arrows match the bullet point numbering below.

- 1) Upon surfacing, the glider calls in to SFMC. Over satellite, it relays status information (time, GPS fix) and transfers scientific data while awaiting instructions as configured by its mission script. The instructions will be received at the last step of this workflow.
- 2) The SFMC Adapter converts the status information and publishes a `platform_status` message to the Communications Backbone message queue.
- 3) The `platform_status` message is delivered to GLAE. The system creates a corresponding problem instance  $I$ .
- 4) The Planner (Algorithm 2) is invoked using the problem instance  $I$ .
- 5) The Simulator (Algorithm 1) is repeatedly called by the Planner. A number of dives on the order of  $10^3 - 10^4$  is simulated by each thread of the Planner. This is the most computationally intensive step, requiring several minutes to complete.
- 6) The best action  $a$  is determined by the Planner and converted to a list of waypoints using Algorithm 3. Corresponding `mission_plan` (the message format representing a waypoint list) and `instruction_set` messages are generated and published to the Communications Backbone.
- 7) The messages are processed by the SFMC Adapter and placed as files in the appropriate directory on SFMC.
- 8) The files are transmitted to the glider and the corresponding parameters are used to execute the next dive.

It is worth reiterating that steps 1 and 8, which involve communication over satellite, are not fully reliable. In preliminary deployments, the rate of successful transfer of waypoint lists and instruction sets was between 88% and 90% overall, with further significant drops during periods with adverse weather conditions. Given that navigation plans cover a longer horizon than individual dives (on the order of a day rather than hours), the glider was able to continue its mission.

## VI. EXPERIMENTAL SETUP

### A. Deployments

Our system was evaluated in two campaigns in the North Sea: *MOGli* (one glider) and *eSWEETS<sup>3</sup>* (two gliders simultaneously). In these deployments, gliders were operated by NOC on behalf of external partners Met Office and the University of East Anglia. A transect formed of two goal positions was used in all deployments. Autonomous control by GLAE was used through the workflows described in the previous section to repeatedly navigate the transects. Deployment coordinates and summary statistics are given in Tables I and II. A map of the three field deployments is shown in Figure 7.

**MOGli.** *Met Office Glider (MOGli)* is an ongoing joint project between the UK Met Office (MO) and NOC. Measurements of ocean properties are gathered by a single glider operated by NOC and transmitted periodically to the MO. This data is used to refine MO models. The use of GLAE to pilot the glider leads to a virtuous circle as AMM15 forecasts are used

TABLE I: Deployment goal locations and parameters. All distances are given in km.

Deployment	Goal 1	Goal 2	Dist.	$\rho$	$\rho_{wpt}$	$n_{bck}$
MOGli	59.32°N 0.35°W	59.32°N 0.65°W	17.0	2.0	7.0	2
eSWEETS <sup>3</sup> N	57.089°N 1.856°W	57.062°N 1.698°W	10.0	1.0	7.0	2
eSWEETS <sup>3</sup> S	56.929°N 1.945°W	56.903°N 1.787°W	10.0	1.0	7.0	2

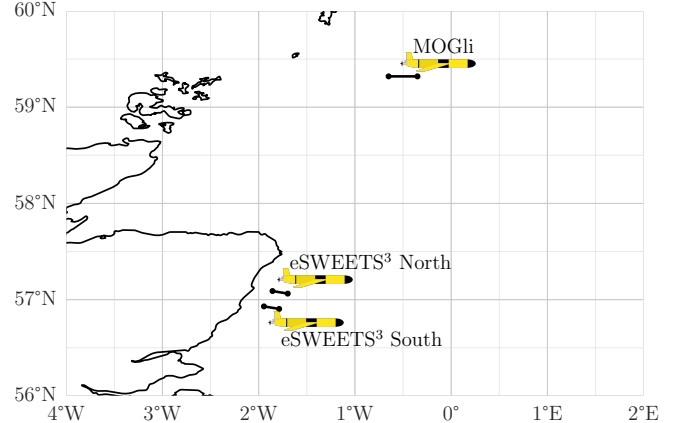


Fig. 7: Locations of the field deployments in the North Sea.

to derive navigation plans, while the scientific data itself is used to improve the forecasts.

For this deployment, a region that exhibits low bottom temperature variance was selected in accordance with the *MOGli* scientific objectives. Fully autonomous control operated from 2 May to 3 July 2025, following preliminary experiments that began in November 2024 and built towards achieving the full glider control loop. A pause in autonomous control was in place from 21 May to 7 June 2025 while the glider was recovered, recharged, and redeployed to the experiment region.

The valid action space allowed relative bearings  $\alpha \in \{-40, -20, 0, 20, 40\}$ . A value of  $n_{yos} = 5$  yos was chosen to lead to an operationally appropriate dive duration (approximately 3 hours). A target depth of  $z_{bottom} = 150$  was used, which exceeds the ocean floor. This was driven by the requirement to sample the entire water column, and hence the glider uses the altimeter to deflect when close to the ocean floor, a feature also supported by our simulator.

**eSWEETS<sup>3</sup>.** In the *enabling Sustainable Wind Energy Expansion in Seasonally Stratified Seas (eSWEETS<sup>3</sup>)* project, two Slocum gliders were deployed around the Kincardine, UK offshore wind farm. The gliders were positioned upstream (referred to as eSWEETS<sup>3</sup> North) and downstream (eSWEETS<sup>3</sup> South) of the wind farm to assess the impacts of the turbine structures on the vertical mixing in the area, which influences oxygen availability, nutrient supplies, and biological productivity.

The project deployments were performed in two phases. In the first phase (May - August 2025), gliders were piloted manually using standard procedures. In the second phase (August - October 2025), GLAE was used to control the gliders

TABLE II: Deployment summary statistics.

Deployment	Transects completed	Duration (days)	Total dives	Distance travelled (km)
MOGLi	41	42	343	665
eSWEETS <sup>3</sup> North	20	27	150	173
eSWEETS <sup>3</sup> South	23	22	147	207

following preliminary experiments and extensions to system functionality. Fully autonomous operation was in place from 2 September to 30 October 2025 for eSWEETS<sup>3</sup> North and from 18 September to 30 October 2025 for eSWEETS<sup>3</sup> South.

The valid action space allowed relative bearings  $\alpha \in \{-90, -60, -30, 0, 30, 60, 90\}$ , a wider range than in MOGLi to account for the strong effect of tidal currents.  $n_{\text{yos}} = 10$  yos were used, leading to dive durations of approximately 4 hours in this shallower region. A target depth of  $z_{\text{bottom}} = 150$  was used which, as in MOGLi, exceeds the bathymetric limit.

The eSWEETS<sup>3</sup> deployments were subject to additional operational requirements. As the gliders were deployed in areas with strong tidal currents, there was a risk of vehicle loss if drifting away from the mission area, especially inland. *Safety polygons* were defined and additional functionality was implemented such that, if the glider drifts outside of the safety polygon, Algorithm 3 is replaced with a simplified navigation plan aiming directly for the center of the polygon. Normal navigation was resumed upon re-entry. Furthermore, as continuing to sample along the transect upon re-entry was deemed more important for the scientific objective than turning back to achieve the goal, the system switched to the next goal if the glider had already progressed past 90% of the transect before exiting the safety polygon.

**Transect integrity.** Occasionally, navigation plans were not generated or followed by the glider due to planned (e.g., software upgrades) or unplanned (e.g., anomalies causing abort of the mission) concerns. Even though these events typically impacted a single surfacing, they compromise the transect validity. Such transects were excluded from the final results.

### B. Simulation Experiments

We present a set of experiments in simulation whose setup mirrors the deployments listed above. They are an idealised version of the real-world experiments, wherein file transfers always succeed and currents experienced are well-represented by the forecasts. Underwater goal achievement detection (Section V-C) and the additional functionality for eSWEETS<sup>3</sup> (Section VI-A) are not supported in simulation. The simulator and planner parameters are otherwise set identically to those used in the field deployments.

We select three scenarios for each deployment to be replayed in simulation. A scenario consists of the starting state (glider position and time) and the goal assigned to the glider in the real world. Scenarios are used as starting conditions for the simulation. To determine the scenarios, we first assess the number of dives required by the Straight-to-Goal method (described in the next subsection) to complete each transect averaged over 200 repetitions. We pick the starting conditions for the transects with the minimum (*Favourable*), median

(*Neutral*), and maximum (*Unfavourable*) dives required, on average, for the baseline to reach the goal. This yields scenarios that represent a range of conditions experienced by the glider during the deployment periods. We then re-run both the Planner and Straight-to-Goal over 1000 random seeds to report the final results.

### C. Baseline

As a baseline for the Planner, we consider the *Straight-to-Goal* approach, which always selects the action with  $\alpha = 0$ . It is used for comparisons in both the simulated and real-world deployments. For an equitable comparison to the Planner, when Straight-to-Goal is used in the real-world deployments, the glider remains under the autonomous control of GLAE.

In the real-world deployments, only one of the two methods can control the glider at any one time. An alternating-control approach was taken, in which Planner and Straight-to-Goal took turns to control the glider after the achievement of 2 goals (equivalently, the algorithm was switched after every back-and-forth transect traversal). Even though the currents experienced by the two algorithms in the real world differ, we expect that any bias thus introduced is removed in expectation. Furthermore, in simulated experiments, we may use the exact same currents when evaluating both methods and replay the same scenarios as many times as desired with different realisations of the uncertainty.

For MOGLi, alternating-control was followed throughout. For eSWEETS<sup>3</sup>, exclusive use of Straight-to-Goal was mandated initially by operational concerns. GLAE was subsequently set to issue Planner waypoints for a comparable duration. For the final period, the algorithms were switched after every transect traversal as in MOGLi.

### D. Metrics

**Planner.** To evaluate the planner, we report the total transect duration (i.e., the cumulative cost as defined in Section IV-B), which is the objective that the method optimises for. As secondary metrics, we report the number of dives (highly correlated with total duration) and the total distance covered for each traversal. All  $\pm$  entries in tables denote 95% confidence intervals.

**Simulator.** To evaluate the simulator, we report the true and simulated dive distances and durations, as well as their differences (deltas). These metrics are assessed on the dives recorded during the live deployment, which were not used for simulator parameter fitting or validation. Furthermore, as the simulator is stochastic and produces several plausible surfacing locations and times, we report statistics with respect to the sample means obtained by drawing 40 samples for each dive.

### E. Simulator and Planner Parameter Optimisation

To optimise the simulator parameters (Section IV-D), we used historical glider states / actions and current forecasts gathered in preliminary deployments (concretely, February - March 2025 for MOGLi and May - June for eSWEETS<sup>3</sup>). We use the files generated by the glider and archived AMM15

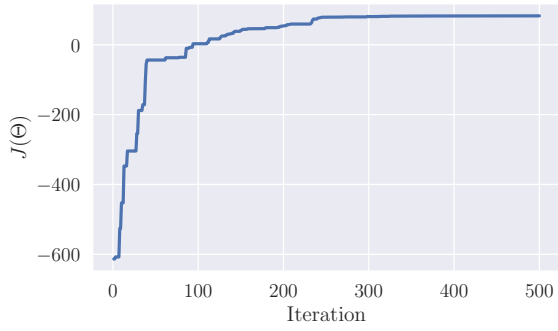


Fig. 8: Learning curve showing the best value of  $J(\Theta)$  found as a function of Bayesian optimisation iterations using the MOGli training data.

forecasts for this purpose. However, such data can also be obtained publicly through the British Oceanographic Data Centre (BODC) [40] and Copernicus [41], with which GLAE is compatible.

The dives are split randomly into training and validation sets. Parameters are optimised using Bayesian optimisation (BO) on the training set, and the best-performing parameters on the validation set with respect to  $J(\Theta)$  are selected. We apply several data cleaning steps by excluding dives that did not terminate due to normal surfacing, those with speed 2 standard deviations outside the mean, and with a difference between heading and surface location greater than a 75 degree threshold.  $n_{\text{SIM-BO}} = 500$  iterations of BO were used as the scoring function plateaued before this step in all experiments.

In terms of planner parameters, we use  $n_{\text{threads}} = 8$  parallel search trees for both deployments. We set  $n_{\text{trials}} = 10000$  and  $n_{\text{trials}} = 5000$  for MOGli and eSWEETS<sup>3</sup> respectively, as for the latter deployment less data is transmitted and therefore less online planning time is available. These parameters are dictated externally by the available resources. We found that the planner hyperparameters (exploration constant, progressive widening parameters, maximum tree depth) are sensitive to simulator parameters. Therefore, after fixing simulator parameters, planner hyperparameters are optimised downstream, also with BO.

## VII. RESULTS

### A. Simulator Evaluation

Figure 8 shows the progress of the scoring function  $J(\Theta)$  during the steps of the Bayesian optimisation procedure on the MOGli data. Several values for the spread penalty  $\lambda_{\text{reg}}$  were tested, and the parameters that obtained the best  $J(\Theta)$  on the validation set were chosen ( $\lambda_{\text{reg}} = 1$  for MOGli, corresponding to the figure shown and  $\lambda_{\text{reg}} = 0$  for eSWEETS<sup>3</sup>).

In Table III, we report several metrics concerning simulator performance on the deployment data (not seen during training or model selection). The distances of the dives output by the simulator were close to their true average on eSWEETS<sup>3</sup>, but noticeably underestimated for MOGli. The distance between the true and simulated surfacing locations is around 1.5 km on average for all deployments (though it is inherently

TABLE III: Comparison of simulated and true dive metrics averaged over all dives executed in the real-world deployments.

Metric	MOGli	eSWEETS <sup>3</sup> North	eSWEETS <sup>3</sup> South
True dive distance (m)	2733	5650	4679
Simulated dive distance (m)	2119	5586	4974
Distance delta (m)	1448	1735	1396
True dive duration (s)	10421	15923	12935
Duration delta (s)	345	1721	1539

TABLE IV: Results comparing the Straight-to-Goal and Planner algorithms across several scenarios in simulation. Bold indicates the better-performing algorithm.

Deployment	Scenario	Algorithm	Mean Duration (hrs)	Mean Number Dives	Mean Transect Length (km)
MOGli	Fav.	STG	22.48 $\pm$ 0.30	7.68 $\pm$ 0.10	17.31 $\pm$ 0.05
		Planner	<b>22.13</b> $\pm$ 0.30	<b>7.57</b> $\pm$ 0.10	<b>16.79</b> $\pm$ 0.06
	Neutral	STG	22.93 $\pm$ 0.31	7.87 $\pm$ 0.11	17.66 $\pm$ 0.05
		Planner	<b>22.38</b> $\pm$ 0.30	<b>7.68</b> $\pm$ 0.10	<b>16.87</b> $\pm$ 0.06
	Unfav.	STG	23.60 $\pm$ 0.34	8.10 $\pm$ 0.12	17.85 $\pm$ 0.06
		Planner	<b>22.84</b> $\pm$ 0.32	<b>7.80</b> $\pm$ 0.11	<b>16.92</b> $\pm$ 0.06
eSWEETS <sup>3</sup> North	Fav.	STG	55.67 $\pm$ 1.40	10.01 $\pm$ 0.26	52.31 $\pm$ 1.54
		Planner	<b>48.70</b> $\pm$ 1.44	<b>8.96</b> $\pm$ 0.28	<b>41.10</b> $\pm$ 1.45
	Neutral	STG	65.70 $\pm$ 0.87	11.33 $\pm$ 0.16	52.92 $\pm$ 1.15
		Planner	<b>62.91</b> $\pm$ 0.92	<b>10.87</b> $\pm$ 0.17	<b>46.67</b> $\pm$ 1.06
	Unfav.	STG	64.07 $\pm$ 1.18	11.79 $\pm$ 0.22	65.20 $\pm$ 1.29
		Planner	<b>55.82</b> $\pm$ 1.43	<b>10.24</b> $\pm$ 0.27	<b>54.57</b> $\pm$ 1.40
eSWEETS <sup>3</sup> South	Fav.	STG	43.46 $\pm$ 1.47	<b>9.70</b> $\pm$ 0.36	43.60 $\pm$ 1.58
		Planner	<b>41.81</b> $\pm$ 1.50	9.78 $\pm$ 0.40	<b>40.09</b> $\pm$ 1.50
	Neutral	STG	55.59 $\pm$ 1.14	11.78 $\pm$ 0.29	53.72 $\pm$ 1.23
		Planner	<b>47.26</b> $\pm$ 0.98	<b>10.07</b> $\pm$ 0.25	<b>43.04</b> $\pm$ 0.95
	Unfav.	STG	61.99 $\pm$ 0.91	13.04 $\pm$ 0.22	68.77 $\pm$ 1.00
		Planner	<b>57.05</b> $\pm$ 1.11	<b>12.52</b> $\pm$ 0.29	<b>59.21</b> $\pm$ 1.12

challenging to draw conclusions by comparing an individual sample with the empirical mean of the simulator distribution). In contrast, the dive durations were more accurate for MOGli, as there is increased variation in the bathymetry between the eastern and western ends of the eSWEETS<sup>3</sup> region.

We note that there are many possible causes for predictive errors in the simulator, which include: forecasts being wrong, the steady-state approximation of our simulator, mismatches between the physical glider used for simulator optimisation and the one used in the real world (distinct vehicles with variations in payload and calibration), and noise in how the glider executes the control commands. It is highly likely that all these factors are at play and, while simulator accuracy can certainly be improved, some degree of error is unavoidable.

### B. Planner Evaluation in Simulation

Table IV shows the results in simulation comparing the Straight-to-Goal and Planner algorithms. The Planner improves over Straight-to-Goal in duration and transect length for all deployments and scenarios, with gains of up to 9.88% and 16.51% respectively. For MOGli, the gains in duration over the baseline are small in an absolute sense at slightly over 30 minutes per transect, equating to a 2.39% decrease. This region does not exhibit strong currents, as corroborated by the small differences in the performance of STG between the most Favourable and Unfavourable scenarios. Therefore,

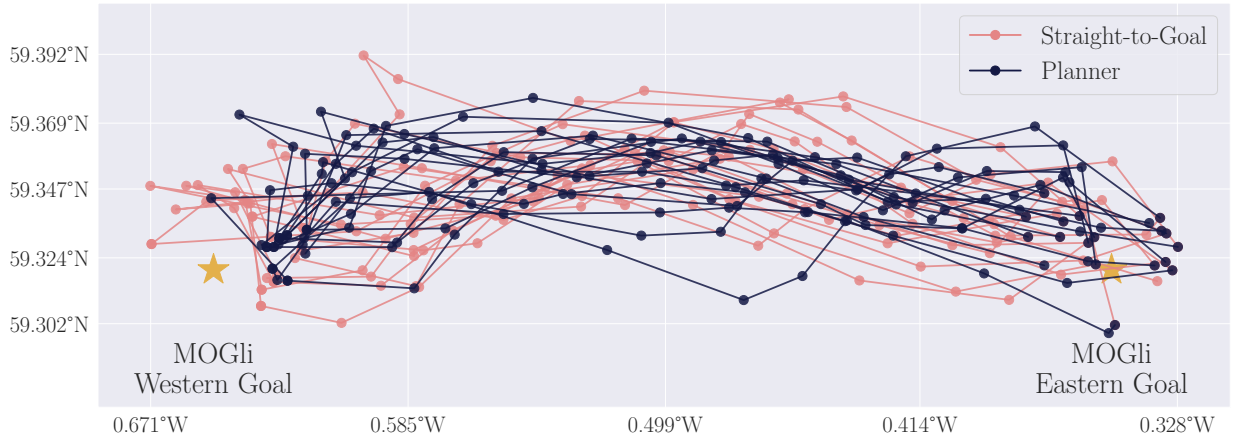


Fig. 9: Transects completed by the proposed GLAE system in the MOGli field deployment using the Planner and the Straight-to-Goal baseline. The Planner results in transects with shorter minimum, mean, and maximum durations. Transects produced by the two methods are also discernible visually. The transects completed by the Planner have statistically significantly shorter distances and avoid overshooting the western goal.

TABLE V: Results comparing the Straight-to-Goal and Planner algorithms in the field deployments. Bold denotes the better-performing algorithm for each deployment and metric.

Deployment	Algorithm	Mean Duration (hrs)	Min Duration (hrs)	Max Duration (hrs)	Mean Number Dives	Min Number Dives	Max Number Dives	Mean Transect Length (km)
MOGli	Straight-to-Goal	23.09	16.00	31.70	8.45	6	11	22.58
	Planner	<b>22.68</b>	<b>14.35</b>	<b>26.98</b>	<b>8.28</b>	<b>5</b>	<b>10</b>	<b>20.52</b>
eSWEETS <sup>3</sup> North	Straight-to-Goal	40.38	19.80	83.54	9.43	5	18	49.10
	Planner	<b>28.88</b>	<b>18.05</b>	<b>43.10</b>	<b>6.46</b>	<b>4</b>	<b>10</b>	<b>38.36</b>
eSWEETS <sup>3</sup> South	Straight-to-Goal	<b>21.37</b>	10.75	54.64	<b>6.00</b>	3	14	<b>29.29</b>
	Planner	26.82	<b>10.44</b>	<b>47.55</b>	7.29	3	<b>13</b>	32.95

our currents-aware approach does not have much room for improvement over this simple algorithm. The gains are more pronounced for eSWEETS<sup>3</sup>, where the Planner leads to decreases of 9.88% and 8.92% respectively in dive duration. The reductions in transect length (of 4.23%, 16.51%, 13.94% for the three deployments) are more pronounced than the duration reductions. This is an important secondary metric as sampling along trajectories that are as straight as possible is key to many scientific objectives.

### C. Planner Evaluation in Field Deployments

Results for the real-world deployments are reported in Table V, showing the Planner outperformed the baseline in 2 out of 3 deployments. For MOGli, as in simulation, the Planner leads to a reduction in the mean duration of approximately 30 minutes on average; the minimum and maximum durations across all transects are also reduced. The Planner yields a reduction in the transect length that is statistically significant at the 5% level ( $p = 0.041$  and rank-biserial  $r = 0.376$  under the nonparametric Mann-Whitney U test with 20 samples for STG and 21 for the Planner). However, given the number of transects recorded (see Table II), statistical significance was not obtained for other deployments and metrics. These field results should be treated as corroborating evidence alongside the larger-scale simulation study rather than as standalone proof of generality.

The Planner also performed better than the baseline for eSWEETS<sup>3</sup> North in all metrics. For eSWEETS<sup>3</sup> South, the mean values for the metrics were slightly worse, while the minimum / maximum ranges still matched or improved over STG. The advantage of the Planner in eSWEETS<sup>3</sup> North is more substantial than that of STG in eSWEETS<sup>3</sup> South.

In Figure 10, we analyse the frequency of the actions taken by the Planner in the three deployments. While the STG action ( $\alpha = 0$ ) is the most selected overall, the Planner chooses to steer frequently. In the eSWEETS<sup>3</sup> region, which is characterised by stronger tidal currents, the distribution of chosen actions is wider and flatter, and even the most extreme actions are still chosen 15% of the time in eSWEETS<sup>3</sup> North. Given this, the Planner could have benefitted from an even wider set of allowed actions in eSWEETS<sup>3</sup> North.

Regarding the alignment between simulation and real-world results, for MOGli, the duration and number of dives are mostly aligned, while the transect lengths are noticeably shorter in simulation. This is consistent with the distance underestimation observed in the simulator evaluation.

For the eSWEETS<sup>3</sup> deployments, values for all metrics were consistently higher in simulation compared to the field deployments. Given the values reported in Section VII-A, simulator predictions of dive distance and durations are well-aligned with field observations. Consequently, the difference in transect metrics is attributable to the goal achievement conditions in the deployed autonomous system being broader (3

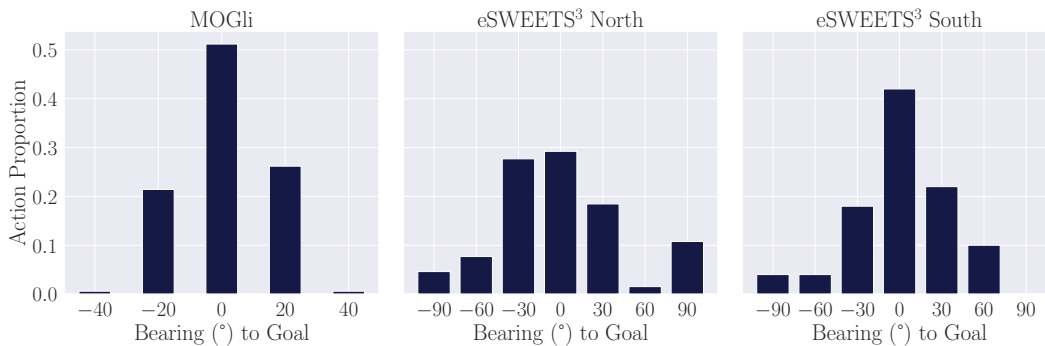


Fig. 10: Proportions of actions chosen by the Planner with respect to the bearing to goal during each of the three field deployments. The stronger currents of the eSWEETS<sup>3</sup> region resulted in a wider distribution of frequencies of chosen actions.

conditions, as described in Sections V-C and VI-A) than those in simulation (1 condition). Requiring surfacing within a tight radius in simulation will result in overshooting the goal and hence longer transects until the goal is eventually achieved. Concretely, the goal was deemed achieved for eSWEETS<sup>3</sup> by reaching it underwater in 43% of cases, having traversed 90% of the transect prior to safety box re-entry in 22% of cases, and by surfacing within the goal radius in only 35% of transects.

### VIII. DISCUSSION

We highlight the following challenges and areas for future work. We aim to generalise our method to also consider the optimisation of energy use, which is feasible with the adopted formulations. As the duration and energy use objectives conflict, a multi-objective approach [42] is required. Extending the method to incorporate constraints and guarantees, such as staying within a specified survey area or avoiding certain areas (e.g., shipping lanes) would broaden the applicability of the method. The problem may also be framed as a POMDP [43] in order to maintain beliefs about the nature of forecast errors, which requires accurate in-situ current measurements.

Replacing or augmenting the simulator with a learned model, which has proven successful with a variety of planning and reinforcement learning approaches [44], [45], may speed up execution and thus enable planning over a longer horizon. As shown by our simulator evaluation, further improvements in accuracy are possible. Fitting simulator behaviours using different vehicles and deployment environments is a significant challenge due to distribution shifts. Further developments to the planner can include the aggregation of continuous actions for root-parallel MCTS [46], improving the exploration strategy [47], and contextually deciding which actions should be prioritised.

Evaluating glider navigation planning algorithms in the field is inherently challenging given the long transect traversals and, consequently, the low number of samples obtained. If resources permit, running algorithms on gliders deployed side-by-side in a paired experimental design would reduce variability and temporal dependencies compared to the alternative-control design we adopted. However, replaying on-field conditions in suitably calibrated simulators, as performed in

our evaluation, is ultimately necessary for statistically robust findings.

Failures in transferring instructions also pose a unique challenge, as they can cause the glider to turn around towards a stale waypoint. Such failures disproportionately impact navigation plans with waypoints that steer away from the goal to compensate for currents. This phenomenon highlights the trade-off between the gains of online planning for steering given up-to-date current forecasts versus the negative impacts of using a stale online plan due to failed instruction transfers. This can be addressed by explicitly reasoning about the time available for planning [48] and limiting it in order to improve the probability of successful transfer.

In terms of applications, we envisage leveraging the present work as a building block. Analysing ocean fronts for features such as temperature [49] or algal blooms [50] can be achieved by creating a higher-level component that reasons about where the highest-value observation(s) can be gathered and tasking the glider accordingly. For going beyond the single-glider scenario, coordination strategies can be considered in a multi-robot setting.

### IX. CONCLUSION

In this paper, we have considered the problem of navigation planning for underwater gliders, an invaluable tool for ocean sampling. We have taken important steps for addressing methodological and systems gaps towards achieving long-term autonomous glider operation. Our work proposed a glider simulator and a procedure for adjusting its parameters using historical dives performed in the real world. We have also contributed a sample-based online planning technique for deciding how to control the robot with the objective of minimising duration to reach the goal. Lastly, in collaboration with pilots and domain experts, we have designed the Glider Long-term Autonomy Engine system, which is suitable for long-term missions. We have thoroughly validated our approach in simulation and through extensive trials in the North Sea. Our work paves the way towards autonomous management of fleets of gliders and can ultimately support advancements in marine science and policy.

## ACKNOWLEDGMENTS

This work was supported by the UK Natural Environment Research Council (NERC) under the UKRI TWINE programme (grant number NE/Z503381/1) and the Doctoral Training Partnership in Environmental Research (NE/S007474/1), the UK Engineering and Physical Sciences Research Council (EPSRC) From Sensing to Collaboration Programme Grant (EP/V000748/1), and the Innovate UK AutoInspect Grant (1004416). The authors would like to gratefully acknowledge the contribution of the Met Office and the University of East Anglia, who gave permission for the GLAE system to be trialled in their glider campaigns. We thank Christopher Auckland & Rob Hall (University of East Anglia), who helped design the additional features for the eSWEETS<sup>3</sup> campaign. Lastly, we acknowledge the use of the University of Oxford Advanced Research Computing (ARC) facility in carrying out this work (see <http://dx.doi.org/10.5281/zenodo.22558>).

## ADDITIONAL INFORMATION

A patent application has been submitted on the work covered in this paper, which was first filed on 19 December 2024 under UK application number GB2418678.5.

## REFERENCES

- [1] D. L. Rudnick, R. E. Davis, C. C. Eriksen, D. M. Fratantoni, and M. J. Perry, "Underwater Gliders for Ocean Research," *Marine Technology Society Journal*, vol. 38, no. 2, pp. 73–84, 2004.
- [2] D. Roemmich, S. Riser, R. Davis, and Y. Desaubies, "Autonomous Profiling Floats: Workhorse for Broad-scale Ocean Observations," *Marine Technology Society Journal*, vol. 38, no. 2, pp. 21–29, 2004.
- [3] D. Roemmich, "On the Future of Argo: A Global, Full-Depth, Multi-Disciplinary Array," *Frontiers in Marine Science*, 2019.
- [4] P. Testor, B. De Young, D. L. Rudnick, S. Glenn, D. Hayes, C. M. Lee, C. Pattiaratchi, K. Hill, E. Heslop, V. Turpin, P. Alenius, C. Barrera, J. A. Barth, N. Beaird, G. Bécu, A. Bosse, F. Bourrin, J. A. Brearley, Y. Chao, S. Chen, J. Chiggiato, L. Coppola, R. Crout, J. Cummings, B. Curry, R. Curry, R. Davis, K. Desai, S. DiMarco, C. Edwards, S. Fielding, I. Fer, E. Frajka-Williams, H. Gildor, G. Goni, D. Gutierrez, P. Haugan, D. Hebert, J. Heiderich, S. Henson, K. Heywood, P. Hogan, L. Houpert, S. Huh, M. E. Inall, M. Ishii, S.-i. Ito, S. Itoh, S. Jan, J. Kaiser, J. Karstensen, B. Kirkpatrick, J. Klymak, J. Kohut, G. Krahnemann, M. Krug, S. McClatchie, F. Marin, E. Mauri, A. Mehra, M. P. Meredith, T. Meunier, T. Miles, J. M. Morell, L. Mortier, S. Nicholson, J. O'Callaghan, D. O'Conchubhair, P. Oke, E. Pallàs-Sanz, M. Palmer, J. Park, L. Perivoliotis, P.-M. Poulain, R. Perry, B. Queste, L. Rainville, E. Rehm, M. Roughan, N. Rome, T. Ross, S. Ruiz, G. Saba, A. Schaeffer, M. Schönau, K. Schroeder, Y. Shimizu, B. M. Sloyan, D. Smeed, D. Snowden, Y. Song, S. Swart, M. Tenreiro, A. Thompson, J. Tintore, R. E. Todd, C. Toro, H. Venables, T. Wagawa, S. Waterman, R. A. Watlington, and D. Wilson, "OceanGliders: A Component of the Integrated GOOS," *Frontiers in Marine Science*, vol. 6, p. 422, 2019.
- [5] H. Stommel, "The Slocum Mission," *Oceanography*, vol. 2, no. 1, pp. 22–25, 1989.
- [6] C. Whitt, J. Pearlman, B. Polagye, F. Caimi, F. Muller-Karger, A. Copping, H. Spence, S. Madhusudhana, W. Kirkwood, L. Grosjean, B. M. Fiaz, S. Singh, S. Singh, D. Manalang, A. S. Gupta, A. Maguer, J. J. H. Buck, A. Marouchos, M. A. Atmanand, R. Venkatesan, V. Narayanaswamy, P. Testor, E. Douglas, S. De Halleux, and S. J. Khalsa, "Future Vision for Autonomous Ocean Observations," *Frontiers in Marine Science*, vol. 7, p. 697, 2020.
- [7] T. Inanc, S. Shadden, and J. Marsden, "Optimal trajectory generation in ocean flows," in *American Control Conference (ACC)*, 2005.
- [8] W. Zhang, T. Inanc, S. Ober-Blobbaum, and J. E. Marsden, "Optimal trajectory generation for a glider in time-varying 2D ocean flows B-spline model," in *International Conference on Robotics and Automation (ICRA)*, 2008.
- [9] D. Kruger, R. Stolkin, A. Blum, and J. Briganti, "Optimal AUV path planning for extended missions in complex, fast-flowing estuarine environments," in *International Conference on Robotics and Automation (ICRA)*, 2007.
- [10] T. Lolla, M. P. Ueckermann, K. Yigit, P. J. Haley, and P. F. J. Lermusiaux, "Path planning in time dependent flow fields using level set methods," in *International Conference on Robotics and Automation (ICRA)*, 2012.
- [11] M. Aguiar, J. B. de Sousa, J. M. Dias, J. E. da Silva, R. Mendes, and A. S. Ribeiro, "Optimizing autonomous underwater vehicle routes with the aid of high resolution ocean models," in *OCEANS*, 2019.
- [12] F. Lekien, L. Mortier, and P. Testor, "Glider Coordinated Control and Lagrangian Coherent Structures," *IFAC Proceedings Volumes*, vol. 41, no. 1, pp. 125–130, 2008.
- [13] N. E. Leonard, D. A. Paley, F. Lekien, R. Sepulchre, D. M. Fratantoni, and R. E. Davis, "Collective Motion, Sensor Networks, and Ocean Sampling," *Proceedings of the IEEE*, vol. 95, no. 1, pp. 48–74, 2007.
- [14] N. E. Leonard, D. A. Paley, R. E. Davis, D. M. Fratantoni, F. Lekien, and F. Zhang, "Coordinated control of an underwater glider fleet in an adaptive ocean sampling field experiment in Monterey Bay," *Journal of Field Robotics*, vol. 27, no. 6, pp. 718–740, 2010.
- [15] E. Fernández-Perdomo, J. Cabrera-Gómez, D. Hernández-Sosa, J. Isern-González, A. C. Domínguez-Brito, A. Redondo, J. Coca, A. G. Ramos, E. Á. Fanjul, and M. García, "Path planning for gliders using regional ocean models: Application of Pinzón path planner with the ESEOAT model and the RU27 trans-Atlantic flight data," in *OCEANS*, 2010.
- [16] W. H. Al-Sabban, L. F. Gonzalez, and R. N. Smith, "Extending persistent monitoring by combining ocean models and Markov decision processes," in *OCEANS*, 2012.
- [17] Mausam and A. Kolobov, *Planning with Markov Decision Processes: an AI Perspective*. Morgan & Claypool Publishers, 2012, vol. 17.
- [18] R. S. Sutton and A. G. Barto, *Reinforcement Learning: An Introduction*. MIT Press, 2018.
- [19] D. Silver and J. Veness, "Monte-Carlo planning in large POMDPs," *Advances in Neural Information Processing Systems*, vol. 23, 2010.
- [20] C. B. Browne, E. Powley, D. Whitehouse, S. M. Lucas, P. I. Cowling, P. Rohlfshagen, S. Tavener, D. Perez, S. Samothrakis, and S. Colton, "A survey of Monte Carlo tree search methods," *IEEE Transactions on Computational Intelligence and AI in Games*, vol. 4, no. 1, pp. 1–43, 2012.
- [21] L. Kocsis and C. Szepesvári, "Bandit based Monte-Carlo planning," in *European Conference on Machine Learning (ECML)*, 2006.
- [22] P. Auer, N. Cesa-Bianchi, and P. Fischer, "Finite-time Analysis of the Multiarmed Bandit Problem," *Machine Learning*, vol. 47, no. 2, pp. 235–256, 2002.
- [23] G. M. J.-B. Chaslot, M. H. M. Winands, and B. Bouzy, "Progressive strategies for Monte-Carlo Tree Search," *New Mathematics and Natural Computation*, vol. 4, no. 03, pp. 343–357, 2008.
- [24] A. Couëtoux, J.-B. Hoock, N. Sokolovska, O. Teytaud, and N. Bonnard, "Continuous Upper Confidence Trees," in *Learning and Intelligent Optimization*, 2011, vol. 6683, pp. 433–445.
- [25] T. Cazenave and N. Jouandeau, "On the Parallelization of UCT," in *Computer Games Workshop*, 2007.
- [26] G. M. J.-B. Chaslot, M. H. M. Winands, and H. J. Van Den Herik, "Parallel Monte-Carlo Tree Search," in *Computers and Games*, 2008, vol. 5131, pp. 60–71.
- [27] J. A. Graham, E. O'Dea, J. Holt, J. Polton, H. T. Hewitt, R. Furner, K. Guihou, A. Brereton, A. Arnold, S. Wakelin, J. M. Castillo Sanchez, and C. G. Mayorga Adame, "AMM15: a new high-resolution NEMO configuration for operational simulation of the European north-west shelf," *Geoscientific Model Development*, vol. 11, no. 2, pp. 681–696, 2018.
- [28] Met Office, "Met office marine data service," <https://www.metoffice.gov.uk/services/data/met-office-marine-data-service>, 2025, accessed: 2025-11-05.
- [29] L. Merckelbach, "glidersim," <https://github.com/smerckel/glidersim>, 2025, accessed: 2025-11-05.
- [30] —, "Depth-averaged instantaneous currents in a tidally dominated shelf sea from glider observations," *Biogeosciences*, vol. 13, no. 24, pp. 6637–6649, 2016.
- [31] L. Merckelbach, A. Berger, G. Krahnemann, M. Dengler, and J. R. Carpenter, "A Dynamic Flight Model for Slocum Gliders and Implications for Turbulence Microstructure Measurements," *Journal of Atmospheric and Oceanic Technology*, vol. 36, no. 2, pp. 281–296, 2019.
- [32] M. Balandat, B. Karrer, D. Jiang, S. Daulton, B. Letham, A. G. Wilson, and E. Bakshy, "BoTorch: A framework for efficient Monte-Carlo Bayesian optimization," in *Advances in Neural Information Processing Systems*, vol. 33, 2020.

- [33] M. Olson, E. Santorella, L. C. Tiao, S. Cakmak, M. Garrard, S. Daulton, Z. J. Lin, S. Ament, B. Beckerman, E. Onofrey, P. Igusti, C. Lara, B. Letham, C. Cardoso, S. S. Shen, A. C. Lin, M. Grange, E. Kashtelyan, D. Eriksson, M. Balandat, and E. Bakshy, "Ax: a platform for adaptive experimentation," in *AutoML 2025 ABCD Track*, 2025.
- [34] D. C. Webb, P. J. Simonetti, and C. P. Jones, "Slocum: An underwater glider propelled by environmental energy," *IEEE Journal of Oceanic Engineering*, vol. 26, no. 4, pp. 447–452, 2001.
- [35] Teledyne Marine, "Slocum glider," <https://www.teledynemarine.com/brands/webb-research/slocum-glider>, 2025, accessed: 2025-12-01.
- [36] C. C. Eriksen, T. J. Osse, R. D. Light, T. Wen, T. W. Lehman, P. L. Sabin, J. W. Ballard, and A. M. Chiodi, "Seaglider: A long-range autonomous underwater vehicle for oceanographic research," *IEEE Journal of Oceanic Engineering*, vol. 26, no. 4, pp. 424–436, 2001.
- [37] C. A. Harris, A. Lorenzo-Lopez, O. Jones, J. J. H. Buck, A. Kokkinaki, S. Loch, T. Gardner, and A. B. Phillips, "Oceanids C2: An Integrated Command, Control, and Data Infrastructure for the Over-the-Horizon Operation of Marine Autonomous Systems," *Frontiers in Marine Science*, vol. 7, p. 397, 2020.
- [38] National Oceanography Centre Marine Autonomous and Robotic Systems Team, "Communications backbone," <https://gitlab.com/nocacuk/mars-oss/cb/communications-backbone>, 2026, accessed: 2026-01-06.
- [39] —, "Backbone message formats," <https://gitlab.com/nocacuk/mars-oss/cb/backbone-message-format>, 2026, accessed: 2026-01-06.
- [40] National Oceanography Centre, "British Oceanographic Data Centre (BODC)," <https://www.bodc.ac.uk/>, 2025, accessed: 2025-11-05.
- [41] Copernicus Authors, "Copernicus Monitoring Environment Marine Service (CMEMS)," <https://marine.copernicus.eu/>, 2025, accessed: 2025-11-05.
- [42] D. M. Roijers, P. Vamplew, S. Whiteson, and R. Dazeley, "A Survey of Multi-Objective Sequential Decision-Making," *Journal of Artificial Intelligence Research*, vol. 48, pp. 67–113, 2013.
- [43] Z. Sunberg and M. Kochenderfer, "Online algorithms for pomdps with continuous state, action, and observation spaces," in *International Conference on Automated Planning and Scheduling (ICAPS)*, 2018.
- [44] D. Hafner, T. Lillicrap, I. Fischer, R. Villegas, D. Ha, H. Lee, and J. Davidson, "Learning latent dynamics for planning from pixels," in *International Conference on Machine Learning (ICML)*, 2019.
- [45] J. Schrittwieser, I. Antonoglou, T. Hubert, K. Simonyan, L. Sifre, S. Schmitt, A. Guez, E. Lockhart, D. Hassabis, T. Graepel, T. Lillicrap, and D. Silver, "Mastering Atari, Go, chess and shogi by planning with a learned model," *Nature*, vol. 588, no. 7839, pp. 604–609, 2020.
- [46] J. Xiao, V.-A. Darvari, B. Lacerda, and N. Hawes, "Gaussian process aggregation for root-parallel monte carlo tree search with continuous actions," *arXiv preprint arXiv:2512.09727*, 2025.
- [47] M. Painter, M. Baoumy, N. Hawes, and B. Lacerda, "Monte Carlo Tree Search with Boltzmann exploration," *Advances in Neural Information Processing Systems*, vol. 36, 2023.
- [48] M. Budd, B. Lacerda, and N. Hawes, "Stop! planner time: Metareasoning for probabilistic planning using learned performance profiles," in *Proceedings of the AAAI Conference on Artificial Intelligence*, 2024.
- [49] Y. Zhang, C. Rueda, B. Kieft, J. P. Ryan, C. Wahl, T. C. O'Reilly, T. Maughan, and F. P. Chavez, "Autonomous tracking of an oceanic thermal front by a Wave Glider," *Journal of Field Robotics*, vol. 36, no. 5, pp. 940–954, 2019.
- [50] J. Fonseca, M. Aguiar, J. B. D. Sousa, and K. H. Johansson, "Algal Bloom Front Tracking Using an Unmanned Surface Vehicle: Numerical Experiments Based on Baltic Sea Data," in *OCEANS*, 2021.